Monthly Notices of the ROYAL ASTRONOMICAL SOCIETY

MNRAS **467,** 428–436 (2017) doi:10.1093/mnras/stx107
Advance Access publication 2017 January 16

Superhumps and spin-period variations in the intermediate polar RX J2133.7+5107

E. de Miguel,[1,2★] J. Patterson,[3★] J. L. Jones,[4] E. Morelle,[5] D. R. S. Boyd,[6] W. Stein,[7] R. Koff,[8] T. Krajci,[9] T. Campbell,[10] G. Roberts,[11] J. Ulowetz,[12] D. Barrett,[13] D. Cejudo,[14] K. Menzies,[15] D. Lemay,[16] J. Rock,[17] R. Sabo[18] and G. Myers[19]

[1]*Departamento de Ciencias Integradas, Facultad de Ciencias Experimentales, Universidad de Huelva, E-21071 Huelva, Spain*
[2]*CBA Huelva, Observatorio del CIECEM, Parque Dunar, Matalascañas, E-21760 Almonte, Huelva, Spain*
[3]*Department of Astronomy, Columbia University, 550 West 120th Street, New York, NY 10027, USA*
[4]*CBA Oregon, Jack Jones Observatory, 22665 Bents Road NE, Aurora, OR 97002, USA*
[5]*CBA France, 9 Rue Vasco de Gama, F-59553 Lauwin Planque, France*
[6]*CBA Oxford, West Challow Observatory, 5 Silver Lane, West Challow OX12 9TX, UK*
[7]*CBA Las Cruces, 6025 Calle Paraiso, Las Cruces, NM 88012, USA*
[8]*CBA Colorado, Antelope Hills Observatory, 980 Antelope Drive West, Bennett, CO 80102, USA*
[9]*CBA New Mexico, PO BOX 1351, Clodcroft, NM 88317, USA*
[10]*CBA Arkansas, 7021 Whispering Pine Road, Harrison, AR 72601, USA*
[11]*CBA Tennessee, 2007 Cedarmont Drive, Franklin, TN 37067, USA*
[12]*CBA Illinois, Northbrook Meadow Observatory, 855 Fair Lane, Northbrook, IL 60062, USA*
[13]*Observatory Le Marouzeau, 6 Le Marouzeau, St Leger Bridereix, F-23300, France*
[14]*CBA Madrid, Camino de las Canteras 42, Buzón 5, La Pradera del Amor, El Berrueco, E-28192 Madrid, Spain*
[15]*CBA Massachusetts, 318A Potter Road, Framingham, MA 01701, USA*
[16]*CBA Quebec, 195 Rang 4 Ouest, St-Anaclet, QC G0K 1H0, Canada*
[17]*CBA Wilts, 2 Spa Close, Highworth, Swindon SN6 7PJ, UK*
[18]*CBA Montana, 2336 Tailcrest Drive, Bozeman, MT 59718, USA*
[19]*CBA San Mateo, 5 Inverness Way, Hillsborough, CA 94010, USA*

Accepted 2017 January 12. Received 2016 December 29; in original form 2016 September 26

ABSTRACT

We report the results of long-term time series photometry on RX J2133.7+5107, an intermediate polar distinguished by its long orbital period (7.14 h) and rapid rotation (571 s) of its white dwarf. The light curves show the presence of a conspicuous modulation with a 6.72-h period, 6.1 ± 0.1 per cent shorter than the orbital period, which we interpret as a (negative) superhump associated with the nodal precession of the accretion disc. This detection may prove a challenge to the idea that superhumps are limited to binaries of short orbital period. Our rotational timings over the 7 yr spanned by our observations show spin-up at a rate of 3.41(2) ms yr^{-1} or, equivalently, on a time-scale $|P/\dot{P}| = 0.17 \times 10^6$ yr. The latter is sensibly shorter than the time-scale of spin period variations reported for other intermediate polars, possibly due to a greater accretion rate.

Key words: accretion, accretion discs – binaries: close – Stars: individual: RX J2133.7+5107 – novae, cataclysmic variables.

1 INTRODUCTION

Large-amplitude light variations at a period slightly displaced from the orbital period were first reported in the cataclysmic variable (CV) VW Hyi during a dwarf-nova eruption (Vogt 1974; Warner 1975). They were known as 'superhumps', partly because they were found to be ubiquitous in the supermaxima of short-period dwarf novae. Eventually a promising theory emerged: the result of a tidally induced instability in the accretion disc (Whitehurst 1988; Hirose & Osaki 1990; Lubow 1991; Whitehurst & King 1991). The cause of this instability is now understood; it is due to the 3:1 resonance between the fluid flow in the outermost parts of the disc and the donor star. The accretion disc is deformed to an eccentric pattern and slowly precesses in the prograde direction in the inertial frame. This naturally accounts for the ∼3 per cent shift from the orbital

★ E-mail: edmiguel63@gmail.com (EdM); jop@astro.columbia.edu (JP)

© 2017 The Authors
Published by Oxford University Press on behalf of the Royal Astronomical Society

Downloaded from https://academic.oup.com/mnras/article-abstract/467/1/428/2908342
by Biblioteca Universitaria de Huelva user
on 11 June 2018

period, $P_{\rm orb}$, since the relevant clock of the superhump phenomenon is determined by the synodic period between the precession and orbital periods.

The 3:1 resonance is crucial in the theory. The tidal instability is only realized when the disc is large enough to accommodate the 3:1 resonance radius, which in turn suggests that superhumps should be limited to a range of mass ratio $q = M_2/M_1 \lesssim 0.25$ (Whitehurst 1988; Hirose & Osaki 1990). Observations are roughly consistent with this, although the upper limit appears to be closer to $q = 0.35$ (Patterson et al. 2005).

Several hundred CVs are now known to show superhumps, and it is now considered a universal characteristic of short-period dwarf novae. An up-to-date elaboration of the theory and observations is presented by Osaki & Kato (2013a). Trust in this enterprise has evolved to the point where the observed period excess of superhump over $P_{\rm orb}$ [$\varepsilon = (P_{\rm sh} - P_{\rm orb})/P_{\rm orb}$] is now considered to be a measure of mass ratio (Patterson et al. 2005; Kato & Osaki 2013a), which is hard to learn in any other way.

In the course of these searches for superhumps and orbital variations, another class of phenomena was discovered: photometric waves with period slightly shorter than $P_{\rm orb}$ (called 'negative' superhumps, since ε is negative). About 20 such stars are now known in the ranks of CVs; a recent survey is given by Armstrong et al. (2013) (see their table 5). The working hypothesis suggested by Barrett, O'Donoghue & Warner (1988) and Harvey et al. (1995) is that these negative superhumps result when the disc comes out of the orbital plane and undergoes *retrograde* precession. As pointed out by Harvey et al. (1995) and Montgomery (2009), it makes a pretty picture: the donor–white dwarf (WD)–disc–particle system mimicking the well-known prograde and retrograde precession in the Sun–Earth–Moon system – even in quantitative detail.

But unlike the situation for positive superhumps, there is still no understanding of which stars engage in negative-superhump theatrics, and which do not. And why. We are still searching for the empirical clues.

In this paper, we report discovery of a new negative superhumper, with $P_{\rm orb}$ longer than any previously found, and about twice as long as anything in the positive-superhump world. We speculate that mass ratio and $P_{\rm orb}$ play little or no role in the excitation of negative superhumps.

2 OBSERVATIONS

RX J2133.7+5107 (hereafter RX2133) was first discovered as an X-ray source in the *ROSAT* Galactic Plane Survey and identified by Motch et al. (1998) as a CV. Subsequent X-ray observations with the *XMM–Newton* satellite suggested classification as an intermediate polar (IP) – a subclass of CVs where the central white dwarf rotates asynchronously with the orbital motion of the binary system [see Patterson (1994) for a review] – based on similarities with other IPs with a strong soft X-ray component in the spectrum, and the presence of strong, rapid X-ray pulses associated with the rotation of the white dwarf (de Martino et al. 2006). Katajainen et al. (2007) also presented polarization evidence suggesting a possible magnetic field.

We made this star a target of the Center for Backyard Astrophysics (CBA), a global network of small telescopes distributed world-wide and mostly operated by dedicated amateur astronomers. The telescopes are small – apertures are typically in the 0.25–0.40 m range – and we therefore carried out time series photometry in white (unfiltered) light to improve signal-to-noise and time resolution. This is of key importance for stars that, like RX2133, are expected to flash high-frequency signals. This practice, however, prevents us from transforming instrumental magnitudes into a standard magnitude system. But our wide-band detectors are expected to yield an effective response peaking near 6000 Å for stars with $(B - V) \approx 0$ (typical for many CVs, mainly nova-likes and outbursting dwarf novae), which makes our unfiltered magnitudes correspond roughly to V light.

Table 1. Log of observations.

Year	JD range (JD – 2400000)	Baseline (d)	Nights/hours
2010	55 461.3–55 507.5	46	27/151.7
2011	55 780.7–55 890.6	72	41/244.9
2012	56 125.4–56 178.5	53	15/127.8
2013	56 536.6–56 655.4	119	30/172.4
2014	56 818.5–56 964.4	146	34/193.7
2015	57 177.5–57 378.4	201	33/200.0
2016	57 524.6–57 639.5	115	29/200.9

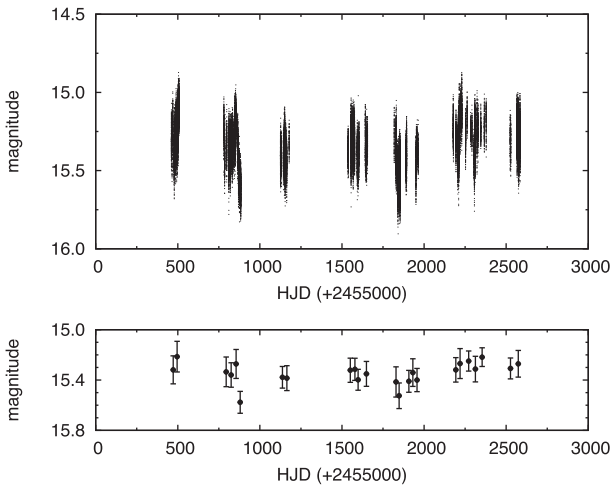

Figure 1. *Upper frame*: The global photometric light curve of RX2133 during 2010–2016. *Lower frame*: Variations of the mean magnitude over stretches of ∼30 d.

Our observations covered all seasons from 2010 to 2016 and consisted of time series with typical time resolution in the range 30–60 s. About two-thirds of these time series were longer than 4 h, while the rest were shorter runs in the 2–4 h range, mainly for the purpose of tracking the spin pulse. A summary of the observing log is given in Table 1. In total, RX 2133 was observed on more than 200 nights, totalling more than 1250 h during 2010–2016.

We used differential photometry with respect to one of the nearby field stars. As differences in spectral response in the equipment are expected, data from different CBA observatories were placed on a common instrumental magnitude scale by adding appropriate offsets. With sufficiently dense coverage and sufficient overlap in the time series, we could establish a consistent calibration of all data from 2010 to 2016, with an expected error in the calibration smaller than 0.1 mag.

The global light curve is shown in the upper frame of Fig. 1. The brightness is seen to vary in the range 15.0–15.7 mag, but there is no discernible long-term pattern in the brightness variations. This is more clearly seen in the bottom frame of Fig. 1, where we show mean magnitudes over ∼30 d stretches. We find that RX2133 remains near 15.3 mag throughout 2010–2016, punctuated by erratic

Downloaded from https://academic.oup.com/mnras/article-abstract/467/1/428/2908342
by Biblioteca Universitaria de Huelva user
on 11 June 2018

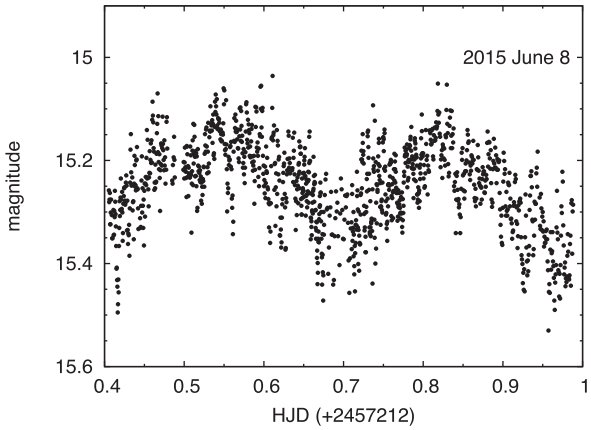

Figure 2. A representative light curve of RX2133 (2015 June 8) showing rapid fluctuations superimposed on a distinct long wave modulation.

changes of 0.2–0.3 mag, perhaps signifying small transient fluctuations in mass-transfer rate.

The 0.7 mag variations seen in the top frame of Fig. 1 are much larger than the dispersion of the mean brightness. These can originate from erratic fluctuations, or possibly from an underlying true periodicity. The light curve shown in Fig. 2 provides a clue. It corresponds to a long data set spanning 14 h, obtained from stations well apart in terrestrial longitude. And it shows rapid variations superimposed on a distinct slow wave. Direct inspection suggests for the latter a roughly 0.3-d time-scale and a full amplitude of ∼0.25 mag. The star repeated this pattern faithfully in all time series of sufficient length (longer than ∼0.3 d) throughout 2010–2016.

3 FREQUENCY ANALYSIS

3.1 Low frequencies

We formed seasonal light curves and analysed them for periodic signals. The frequency analysis was performed by using the PERIOD04 package (Lenz & Breger 2005), based on the discrete Fourier transform method. Uncertainties in the frequencies and amplitudes were estimated by using Monte Carlo methods from the same package. Frequencies are expressed in units of cycles d^{-1}.

The low-frequency region of the power spectrum is shown in Fig. 3. The spectra are dominated by a peak centred at frequency $f \approx 3.57$ cycles d^{-1}, neatly visible in all seasons. There are a number of peaks flanking the dominant signal, and extending towards higher frequencies, but they are all either 1-d aliases of the fundamental signal, or simply noise. This was assessed by removing the dominant signal from the data and re-analysing the residual light curves. Fig. 4 shows an example of this practice for the 2014 data set. The residual spectrum – shown in the lower part of Fig. 4 at the same scale as the main spectrum – is essentially structureless, demonstrating that the 3.57 cycles d^{-1} signal is the only significant feature at these frequencies.

The seven seasonal (yearly) values of the frequency are collected in Table 2. They are roughly consistent with each other, but the precise values differ by amounts exceeding 7σ. The mean value of 3.5685 cycles d^{-1} differs by a whopping 6.1 ± 0.1 per cent from the precise orbital frequency of the binary ($f_{\rm orb} = 3.3621$ cycles d^{-1}; Thorstensen, Peters & Skinner 2010). These two traits of the frequency – exceeding $f_{\rm orb}$ by a few per cent, and varying slightly

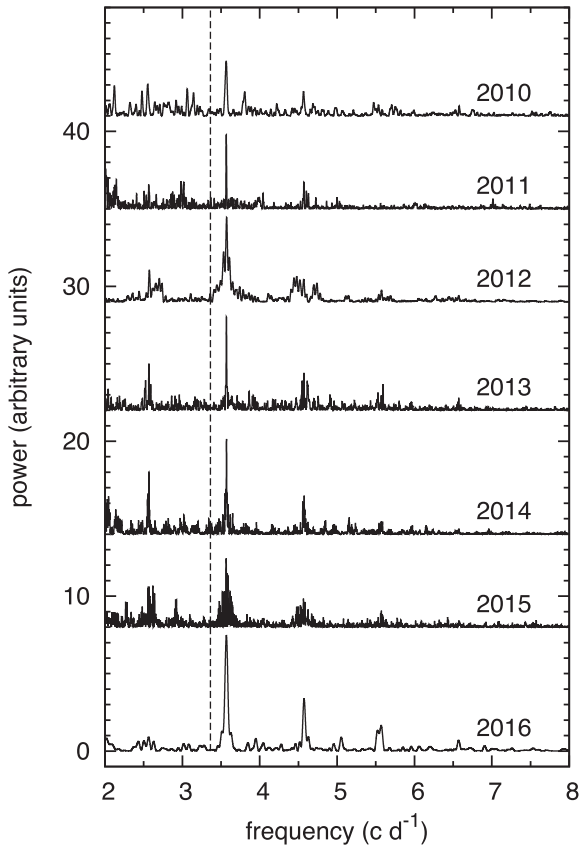

Figure 3. The seasonal power spectrum of RX2133 in the low-frequency region. The power is expressed in arbitrary units. The dashed vertical line shows the expected location of the orbital frequency ($f_{\rm orb} = 3.3621$ cycles d^{-1}).

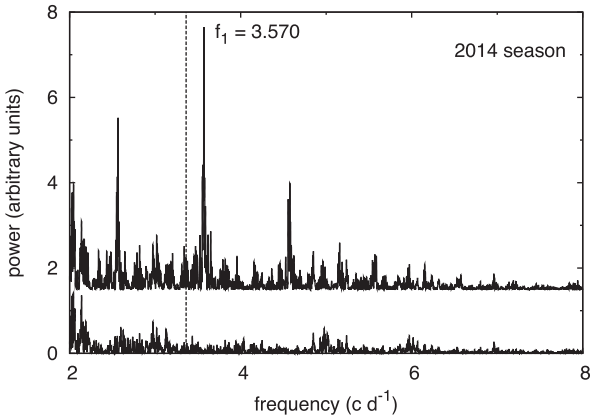

Figure 4. The 2014 power spectrum of RX2133 in the low-frequency region, with the dominant signal (f_1) labelled by its frequency in cycles d^{-1}. The power is in arbitrary units, and the spectrum has been shifted upwards for clarity. The lower part shows the power spectrum of the residual light curve after removal of the f_1 signal. The dashed vertical line shows the expected location of the orbital frequency ($f_{\rm orb} = 3.3621$ cycles d^{-1}).

from year to year – are the defining features of negative superhumps in CVs. RX2133 shows a strong negative superhump.

Better insight on the superhump's stability might be gained by tracking the time evolution of a well-defined feature in the signal, here taken to be the epoch of maximum light. This was easily identified in many nightly light curves, but only those with good

Downloaded from https://academic.oup.com/mnras/article-abstract/467/1/428/2908342
by Biblioteca Universitaria de Huelva user
on 11 June 2018

Table 2. The yearly values of the frequency and semi-amplitude of the superhump modulation. Errors in the semi-amplitudes vary between 1 and 3 mmag.

Year	f_1 (cycles d^{-1})	A_1 (mmag)
2010	3.5677(4)	58
2011	3.5673(2)	72
2012	3.5711(5)	74
2013	3.5698(2)	76
2014	3.5703(2)	78
2015	3.5665(2)	68
2016	3.5666(3)	84

Table 3. Seasonal linear ephemeris of the superhump signal (maximum light); N is the number of timings.

Year	N	frequency (cycles d^{-1})	Zero-point (HJD – 2400000)	rms (d)
2010	12	3.5680(13)	55465.434(12)	0.013
2011	17	3.5675(4)	55780.864(7)	0.012
2012	13	3.5706(11)	56125.568(9)	0.011
2013	16	3.5696(5)	56552.488(4)	0.010
2014	14	3.5700(3)	56827.864(4)	0.009
2015	17	3.5670(2)	57194.563(5)	0.013
2016	18	3.5664(11)	57566.840(6)	0.018

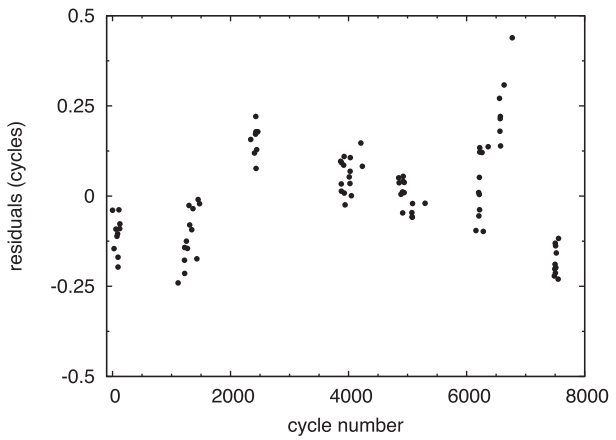

Figure 5. A tentative O–C diagram of the timings of superhump maxima from 2010 through 2016, relative to the test frequency 3.5694 cycles d^{-1}.

sampling at both sides of the maxima (typically ±0.10 d) were tagged for analysis, yielding a total of 107 maxima. Times of maximum light were obtained by fitting a quadratic polynomial to the data. The mean 2σ errors in these timings is ±0.005 d. A linear ephemeris was then determined for each season, with the results summarized in Table 3. The resulting frequencies are consistent with those determined from the Fourier analysis. This is reassuring, since timing the extrema inevitably conveys some arbitrariness in the fitting procedure. The mean frequency throughout 2010-2016 is 3.5684(15) cycles d^{-1}, in full agreement with the mean value found from the Fourier analysis, 3.5685(17) cycles d^{-1}.

Fig. 5 shows the residuals of light maxima from a constant-period fit embracing all seasons ('O–C diagram'). The test frequency was 3.5694 cycles d^{-1}, a value for which the rms scatter of the

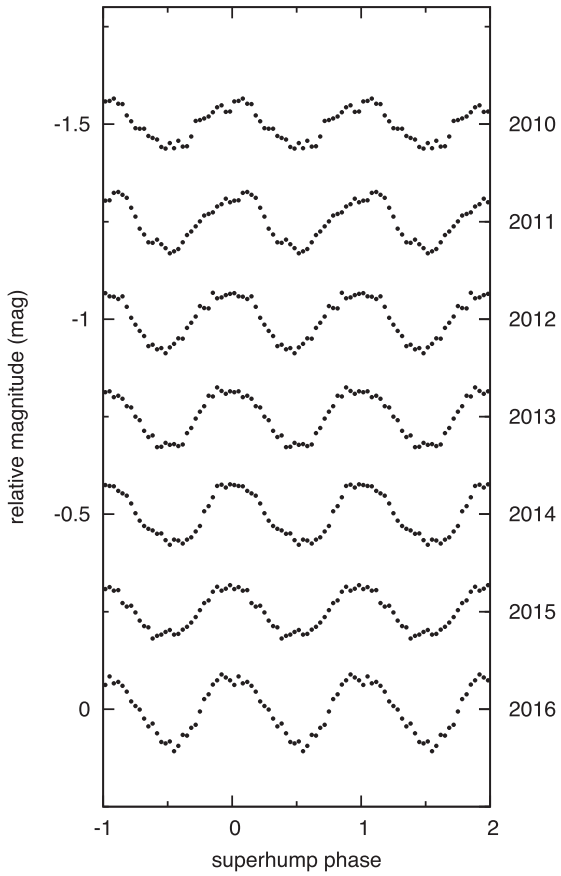

Figure 6. The waveform of the low-frequency signal (superhump) from 2010 (top) to 2016 (bottom). The origin of phase corresponds to maximum light.

residuals was found to have an absolute minimum. The phase is seen to wander by about ±0.1 cycles in every season, and more than twice as much through 2015, the year when our observations spanned the longest baseline. Despite the relatively large phase variations, the observations were well distributed and there were no cycle count problems *during each season*. But some degree of ambiguity was inevitable when connecting consecutive seasons. The O–C diagram in Fig. 5 is simply a tentative representation of the long-term variation of the residuals. The main point here is simply to emphasize again that the underlying clock is not fully stable; and for the most likely cycle count, the variations in the periodicity are non-monotonic and change sign.

The mean waveform of the superhump signal from 2010 through 2016 is shown in Fig. 6. In each case, the data were folded on the mean seasonal period, and aligned on the time of maximum light, which defines phase zero. The waveforms are roughly similar in all seasons.

The expected precession period of the accretion disc is ∼4.8 d, but we do not find any significant detection in the power spectra around the corresponding frequency, with a non-detection limit of ∼0.02 mag. This signal is displayed by some negative superhumpers (Armstrong et al. 2013), and is typically attributed to modulations due to varying projected surface area of the tilted accretion disc during the precession cycle. Its absence in RX2133 may indicate a binary of low inclination.

Downloaded from https://academic.oup.com/mnras/article-abstract/467/1/428/2908342
by Biblioteca Universitaria de Huelva user
on 11 June 2018

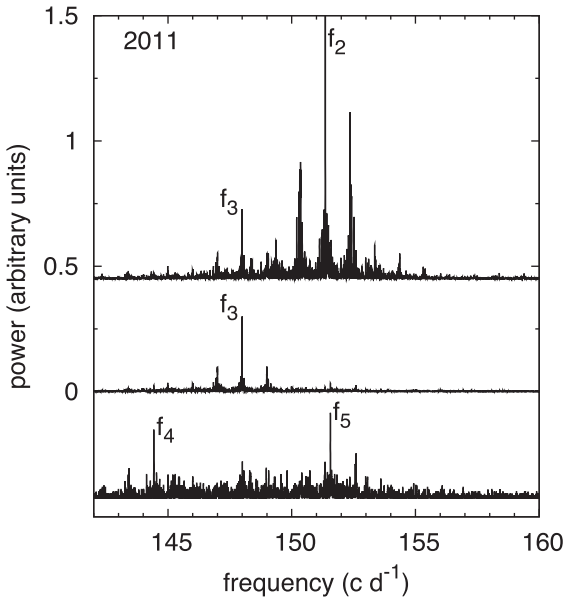

Figure 7. The 2011 power spectrum of RX2133 in the high-frequency region. The upper spectrum is dominated by the spin signal at $f_2 = 151.3583(2)$ cycles d^{-1}, which rises off-scale. The signal at $f_3 = 147.9955(5)$ cycles d^{-1} corresponds to the orbital side-band. The middle spectrum shows f_3 (at the same power scale) after removing the spin signal. Two additional features, $f_4 = 151.564(1)$ cycles d^{-1} and $f_5 = 144.427(2)$ cycles d^{-1} are apparent in the spectrum shown at the bottom (power scale amplified by a factor of 9), obtained after further removing the side-band frequency f_3.

3.2 High frequencies

On every night, the star exhibited a powerful 9.5 min signal in the light curve, with an essentially constant semi-amplitude (∼45 mmag) and significant coherence. For the search of periodic signals in the high-frequency region, we first removed the superhump modulation from the yearly light curves. Fig. 7 shows the high-frequency power spectrum from year 2011. We interpret the dominant signal at $f_2 = 151.3583(2)$ cycles d^{-1}, or 570.8309(8) s, as the optical signature of the spin signal, an interpretation consistent with previous determinations of the spin period from X-rays (570.862 ± 0.034 s; de Martino et al. 2006; Anzolin et al. 2009) and optical observations (570.823 ± 0.013 s; Bonnet-Bidaud et al. 2006). The spin signal is flanked by the usual 1 cycles d^{-1} alias peaks, but the light curve is densely covered from a wide range of terrestrial longitudes, which subdues problems of aliasing. The signal exhibited a semi-amplitude of 45 ± 2 mmag.

The spectrum shows another peak at $f_3 = 147.9955(5)$ cycles d^{-1} and semi-amplitude of 18 ± 2 mmag, unrelated to the alias pattern or the windowing of the observations. The signal becomes more apparent after removal of the dominant spin signal. The resulting spectrum of the residual light curve is shown in the middle frame of Fig. 7. The peak is red-shifted by 3.3628(7) cycles d^{-1} from the spin frequency. Recalling that $f_{\rm orb} = 3.3621$ cycles d^{-1} (Thorstensen et al. 2010), we interpret f_3 as a signature of the lower orbital side-band of the spin frequency – sometimes called the 'beat frequency'. This is a typical feature in IP stars, and is usually interpreted as optical emission from the reprocessing of X-rays in structures fixed in the orbital frame of the binary.

The power spectrum shows two additional small peaks with semi-amplitudes of 6 ± 1 mmag, seen in the lower frame of Fig. 7, obtained after further subtraction of the orbital side-band f_3.[1] These additional detections are centred at $f_4 = 151.564(1)$ and $f_5 = 144.427(2)$ cycles d^{-1} and are faithfully consistent with the combinations $(f_{\rm sp} - f_{\rm orb}) + f_{\rm nsh}$ and $(f_{\rm sp} - f_{\rm orb}) - f_{\rm nsh}$, respectively, where $f_{\rm nsh}$ is the frequency of the negative superhump. The f_4 and f_5 signals are also detected when the light curve is pre-whitened by removing the dominant signals in flux (rather than magnitude) units.

The interpretation of these signals is not straightforward. They involve the superhump signal, which we have shown previously is intrinsically unstable, and therefore may inject some spurious detections. But subtle interactions among different signals may give rise to non-trivial side-band signals in IPs (Warner 1986). A plausible interpretation is that they are the result of amplitude modulation of the side-band on the superhump signal.

The power spectra for all other years were very similar to those depicted in Fig. 7 for 2011. The values of the frequencies varied just slightly from year to year, but the overall pattern remained substantially unchanged.

We also searched for possible detections of harmonics of the main high-frequency signals. Using all data sets, we could only find a spike at 302.7183(1) cycles d^{-1} with a semi-amplitude of 1.3 ± 0.4 mmag barely standing above the background noise (∼0.5 mmag in this frequency region). The optical spin signal is highly sinusoidal.

We note that the orbital motion did not leave a *direct* footprint in our photometry: no signal was found in the power spectra at the orbital frequency within the detection limit of ∼0.03 mag typically found in this frequency regime. Of course it did appear indirectly, since the side-band labelled 'orbital' is likely a proxy for the true orbital frequency. The inferred values yield an average value of $f_{\rm orb} = 3.3621(7)$ cycles d^{-1} or $P_{\rm orb} = 7.1384(15)$ h, in full agreement with the spectroscopic values of 3.36212(6) cycles d^{-1} or 7.13834(12) h, respectively (Thorstensen et al. 2010).

Table 4 presents a summary of the frequencies and amplitudes of these signals.

4 LONG-TERM VARIATION OF THE SPIN PERIOD

Inspection of the entries in Table 4 suggests that the spin frequency is increasing slowly with time. Fig. 8 shows this trend, and the straight-line fit corresponds to spin-up at a rate of 3.8 ± 0.3 ms yr^{-1}. The accuracy of these measurements is sufficiently high, and the signal sufficiently stable, that we can count cycles from year to year. We extracted 239 times of maximum light, with estimated errors in the range 15–40 s.[2] The residuals of these timings are shown in Fig. 9, relative to a constant frequency of 151.359 91 cycles d^{-1}. A parabolic fit of the data yields

$$\mathrm{HJD}_{\rm max}(\mathrm{spin}) = 2455461.39664(4) + 0.0066068819(6)\ E - 3.57(2) \times 10^{-13}\ E^2, \quad (1)$$

with an rms residual of 0.04 cycles (22 s). From the above ephemeris for the spin pulse, we derive $\mathrm{d}P_{\rm sp}/\mathrm{d}t = -3.41(2)$ ms yr^{-1}, which

[1] We note that successive pre-whitening of the light curve may inject unwanted effects in the analysis, particularly if the removed signals wander in phase and/or amplitude. But the spin and orbital side-band signals are expected to be largely stable over each season, and probably the successive whitening procedure used here is warranted.

[2] A table with all these timings is available in the online journal.

Downloaded from https://academic.oup.com/mnras/article-abstract/467/1/428/2908342
by Biblioteca Universitaria de Huelva user
on 11 June 2018

Table 4. The most significant high-frequency detections, along with their semi-amplitudes. The last column includes the *inferred* orbital frequency (see text for details). Errors in the semi-amplitudes vary between 1 and 2 mmag. The last row gives our interpretation of the various frequencies, with the subscripts meaning: negative superhump (nsh), spin (sp) and orbital (orb).

Year	f_2 (cycles d^{-1})	A_2 (mmag)	f_3 (cycles d^{-1})	A_3 (mmag)	f_4 (cycles d^{-1})	A_4 (mmag)	f_5 (cycles d^{-1})	A_5 (mmag)	orbital (cycles d^{-1})
2010	151.3563(6)	44	147.9929(16)	15	151.561(5)	6	144.423(4)	6	3.3634
2011	151.3583(2)	45	147.9955(5)	18	151.564(1)	6	144.427(2)	6	3.3628
2012	151.3591(3)	46	147.9979(9)	14	151.567(3)	5	144.423(2)	5	3.3612
2013	151.3600(1)	47	147.9982(4)	10	151.568(1)	6			3.3618
2014	151.3606(1)	53	147.9987(5)	14	151.569(1)	10	144.429(1)	5	3.3619
2015	151.3618(1)	45	147.9996(2)	17	151.567(1)	9	144.433(1)	6	3.3622
2016	151.3626(1)	47	148.0011(3)	18	151.566(1)	9	144.437(2)	6	3.3615
	f_{sp}		$f_{sp} - f_{orb}$		$(f_{sp} - f_{orb}) + f_{nsh}$		$(f_{sp} - f_{orb}) - f_{nsh}$		f_{orb}

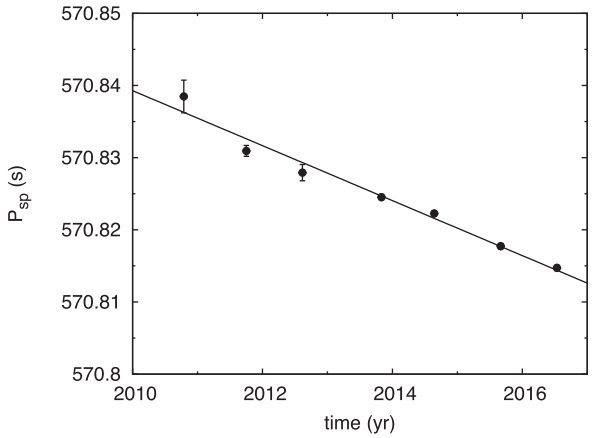

Figure 8. Seasonal values of the spin period P_{sp} during the 2010–2016 campaign. The curve represents a linear fit, which suggests that P_{sp} decreases at a rate of 3.8 ms yr^{-1}.

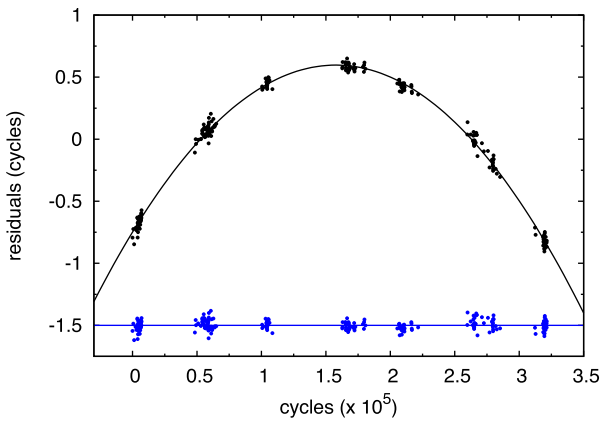

Figure 9. The O–C diagram of the spin pulse maxima over 2010–2016 relative to a linear test ephemeris with $f_{sp} = 151.35991$ cycles d^{-1}. The curve corresponds to the best parabolic fit to the data, giving a decrease rate of 3.41(2) ms yr^{-1} for the spin pulse. The lower part of the figure (blue points) shows the residuals of the pulse timings relative to the parabolic ephemeris given in equation (1).

suggests that the spin period decreases on a characteristic time-scale $|P_{sp}/\dot{P}_{sp}| = 0.17 \times 10^6$ yr.

The good fit of the spin-up ephemeris is obvious in Fig. 9. The seasonal waveforms of the spin signal are also nearly sinusoidal and quite stable, and these are illustrated in Fig. 10.

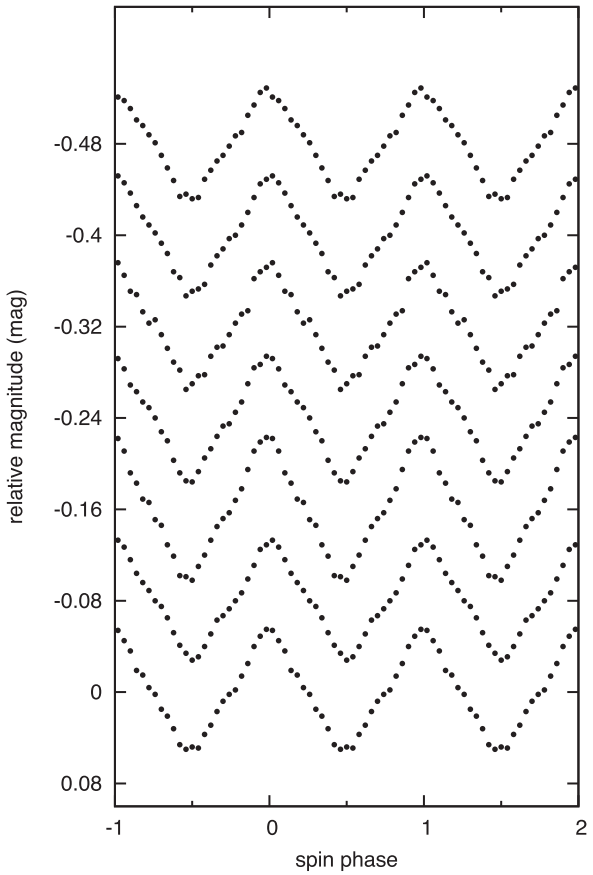

Figure 10. Waveform of the spin pulse from 2010 (top) to 2016 (bottom). The data have been folded according to the quadratic ephemeris given in equation (1). Each data set is shifted 0.08 mag along the vertical axis for clarity.

5 DISCUSSION

5.1 The superhumps

Positive superhumps were first detected in the superoutbursts of short-period dwarf novae, and have become a more or less defining feature of the SU UMa class. Roughly 200 superhumping CVs are now known, and they appear to obey a simple empirical rule: they are seen in nearly all CVs with $P_{orb} < 4$ h and high accretion rates, as long as those rates remain sufficiently high for sufficiently long. For all stars of the SU UMa class, this criterion includes all superoutbursts and excludes all normal outbursts, as required by

Downloaded from https://academic.oup.com/mnras/article-abstract/467/1/428/2908342
by Biblioteca Universitaria de Huelva user
on 11 June 2018

observation. The 4-h cutoff properly includes many nova-like variables, and properly excludes all stars of significantly longer period. This dependence on $P_{\rm orb}$ could also be expressed by stipulating a dependence on mass ratio $q = M_2/M_1 < 0.35$ (Patterson et al. 2005).

Negative superhumpers are much rarer. The combined lists of Montgomery (2009) and Armstrong et al. (2013) show only 23, after a few poorly credentialed stars are dismissed from the former list. A few more recent discoveries have swelled the list to more than 30: V455 And (Kozhevnikov 2015), ER UMa (de Miguel et al. 2012; Oshima et al. 2012, 2014), V1504 Cyg (Osaki & Kato 2013a), VW Hyi (Kato et al. 2014b), KIC 7524178 (Kato & Osaki 2013b), TY PsA (Kato et al. 2014a), V344 Lyr (Osaki & Kato 2013b), 1RXS J003828.7+250920 (Pavlenko et al. 2016), MN Dra (Pavlenko et al. 2010), KIC 8751494 (Kato & Osaki 2013), V378 Peg (Ringwald et al. 2012), V380 Oph (Shugarov et al. 2005), V1101 Aql (de Miguel et al., in preparation), UX UMa (de Miguel et al. 2016) and KIC 9406652 (Gies et al. 2013). Like their better-known cousins, the periods are displaced from $P_{\rm orb}$ by a few per cent, and the exact values wander slightly on a time-scale of weeks to months. RX2133's wandering in phase, seen in Fig. 5, is typical of the class.

What is not typical of the class, so far, is the presence of superhumps in a star of such long orbital period (7.14 h). Of all the class members, only three have $P_{\rm orb} > 0.2$ d: TV Col, at 0.229 d (Bonnet-Bidaud, Motch & Mouchet 1985); KIC 9406652, at 0.254 d (Gies et al. 2013); and RX2133, at 0.297 d. TV Col and RX2133 are both magnetics, and are the only negative superhumpers with solid magnetic credentials. What lessons might lurk in this (arguable) oddity?

The simplest and obvious lesson is that the negative superhump, a phenomenon of accretion discs, does not require a full accretion disc. The truncated disc characteristic of most or all IPs is apparently sufficient.

Another lesson might be that magnetism can increase the outer radius of the truncated discs. The tidal torque, which is thought to drive the precession (e.g. Montgomery 2009), is much greater in the outer disc: the bigger the disc, the stronger the perturbation. An upper limit for the outer edge of a quasi-steady disc is provided by the tidal truncation radius, $R_{\rm tidal}$. In units of the orbital separation, a, an appropriate approximation for $R_{\rm tidal}$ is given by

$$\frac{R_{\rm tidal}}{a} = \frac{0.6}{(1+q)}, \qquad (2)$$

which shrinks to ∼0.4 for the values of q appropriate for long-period CVs. Magnetism may increase this number to ∼0.6 and therefore accommodate larger discs.

On the other hand, the correct lesson might simply be that long-period CVs are few in number (true), and detection of periodic signals at long periods is more difficult (also true). IPs get more attention, since they are rare and somewhat glamorous. Sometimes the anomalies come from the humans, not the physics.

5.2 The spin signals

The family of periodic signals in RX2133 is pretty normal for the IPs: the spin signal, its lower orbital side-band, and various harmonics and side-bands. The spin period of 571 s is also typical of the class.

The observed rate of spin-up (3.4 ms yr^{-1}) is surprisingly fast – apparently the fastest of all known IPs. To study this, we compiled Table 5, containing period and spin-up data for all IP stars with well-measured spin-up rates or limits.

Table 5. Spin-rate changes for IP stars with well-measured spin-up rates or limits.

Object	$P_{\rm spin}$ (s)	$P_{\rm orb}$ (d)	$-\dot{P}_{\rm spin}$	$P_{\rm spin}/\lvert\dot{P}_{\rm spin}\rvert$ (yr)	Refs
V455 And	67.6	0.05631	$<1.1 \times 10^{-14}$	$>2 \times 10^{8}$	1,2
HT Cam	515	0.05971	$<3 \times 10^{-13}$	$>5 \times 10^{6}$	3,4
DW Cnc	2314	0.05979	$<1.5 \times 10^{-12}$	$>5 \times 10^{7}$	4,5
EX Hya	4022	0.06823	4×10^{-11}	3.2×10^{6}	6,7
V515 And	465	0.11379	2.4×10^{-11}	6.1×10^{5}	4,8
BG CMi	913	0.13475	5×10^{-11}	5.8×10^{5}	4,9
V647 Aur	933	0.14402	1.3×10^{-10}	2.4×10^{5}	4,10
V533 Her	63.6	0.1470	$<5 \times 10^{-13}$	2.4×10^{5}	4,11
AO Psc	805	0.14962	6×10^{-11}	4.2×10^{5}	12,13
IGR J16547-1916	546	0.1548	5×10^{-11}	3.5×10^{5}	4,14
V418 Gem	480	0.18205	3×10^{-12}	5×10^{6}	15
DQ Her	71.1	0.19362	5×10^{-13}	4.5×10^{6}	16
FO Aqr	1254	0.20206	8×10^{-11}	5.0×10^{5}	4,17
V667 Pup	512	0.2335	4.8×10^{-11}	3.4×10^{5}	4,18
RX J2133.7+5107	571	0.29743	1.1×10^{-10}	1.7×10^{5}	19
GK Per	351	1.996	1×10^{-11}	10^{6}	20

References. (1) Araujo-Betancor et al. (2005). (2) Mukadam et al. (2016). (3) Kemp et al. (2002). (4) CBA (unpublished). (5) Patterson et al. (2004). (6) Hellier & Sproats (1992). (7) Mauche et al. (2009). (8) Butters et al. (2008). (9) Hellier (1997). (10) Gänsicke et al. (2005). (11) Patterson (1979). (12) Patterson & Price (1981). (13) Kaluzny & Semeniuk (1988). (14) Scaringi et al. (2011). (15) Patterson et al. (2011). (16) Patterson, Robinson & Nather (1978). (17) Patterson et al. (1998). (18) Butters et al. (2007). (19) this paper. (20) Mauche (2004).

To first order, the physics of spin-rate change in a truncated disc should be simple. Matter at the inner edge of the disc, $R_{\rm in}$, carries a specific angular momentum of $R_{\rm in}^2\Omega_{\rm in}$ – where $\Omega_{\rm in}$ is the Keplerian angular velocity at $R_{\rm in}$ – and the WD rotates with a specific angular momentum of $\sim 0.2 R_{\rm WD}^2 \Omega_{\rm WD}$, appropriate for a WD of mass $\sim 0.7\,{\rm M}_\odot$ (Ritter 1985). Accretion can occur whenever $\Omega_{\rm in}$ equals or exceeds $\Omega_{\rm WD}$, and all such cases should result in spin-up, since 1 exceeds 0.2 and $R_{\rm in}$ exceeds $R_{\rm WD}$. Most IPs show a luminous hard X-ray component, suggesting radial infall from a height of at least several WD radii, and probably $R_{\rm in} > 3R_{\rm WD}$.

Two very simple principles should apply. Spin-up is faster for slowly rotating WDs, and for high accretion rates. The vagaries of magnetic fields probably play a very significant role; but with the stars ranging over a factor of 70× in both spin period and likely accretion rate, it is reasonable to inquire if we can learn accretion rates from rates of spin-up.

Most of these accreting stars are probably 'slow rotators', in the sense defined by Ghosh & Lamb (1979). Such stars are spun-up by the accretion torque alone, unmitigated by magnetic field lines dragging in the outer disc. In that case, the spin-up rate is given by equation 18 in Patterson (1994):

$$\dot{P} = -1.7 \times 10^{-11} \mu_{32}^{4/7} M_1^{1.0} P_{1000}^2 \dot{M}_{17}^{6/7} n(\omega_{\rm s}). \qquad (3)$$

Here, $n(\omega_{\rm s})$ is the dimensionless torque function, for which we adopt $n(\omega_{\rm s}) = 1.4$, appropriate for slow rotators. In equation (3), μ_{32} is the magnetic moment of the WD expressed in units of 10^{32} G cm^3, M_1 is the mass of the WD in solar masses, P_{1000} is the spin period in units of 1000 s and $\dot{M}_{17}$ is the accretion rate in units of 10^{17} g s^{-1}. We adopt $\mu_{32} = 1$ and $M_1 = 1$, and use the measured spin-up rates to constrain $\dot{M}$. Specifically, we present in Table 5 the measured values of spin period, its rate of change and orbital period. Then in Fig. 11,

Downloaded from https://academic.oup.com/mnras/article-abstract/467/1/428/2908342
by Biblioteca Universitaria de Huelva user
on 11 June 2018

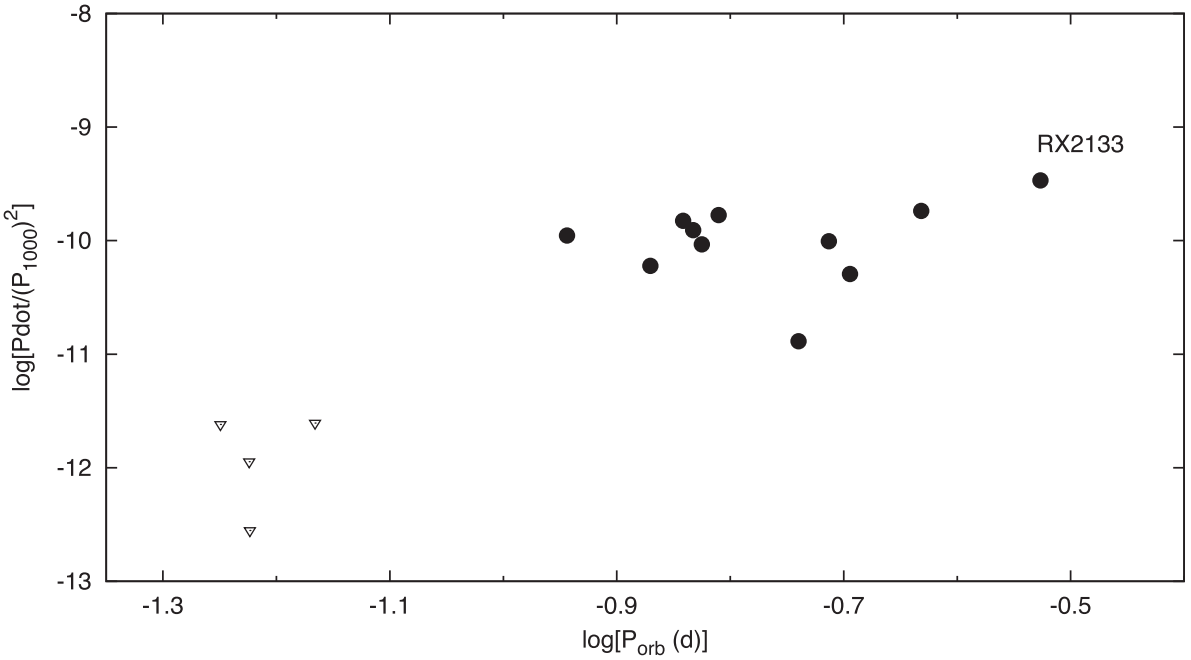

Figure 11. $\dot{P}/P_{1000}^2$ versus $P_{\rm orb}$ for IP stars with well-measured spin-up rates (circles) or upper limits (triangles).

we plot $\dot{P}/(P_{1000})^2$ versus $P_{\rm orb}$ expressed in days.[3] The absence of stars near $\log P_{\rm orb} = -1$ (with the sole exception of V515 And) reflects the well-known 'period gap' in CVs – the extreme scarcity of stars with orbital periods in the range 2–3 h.

Most of the short-period stars have extremely stable periods; no change is yet measured, even on long baselines. The one positive measurement brings the average up to $\sim 10^{-12}$. The long-period stars show a greater spread, with an average near 10^{-10}. The 100× separation between the two classes is very distinct.

We could go one step further and use equation (3) to estimate the accretion rates. Adopting mean values of 8×10^{-13} and 8×10^{-11} for the two classes, equation (3) yields accretion rates of 4.4×10^{-11} and $9.7 \times 10^{-9}\,{\rm M}_\odot\,{\rm yr}^{-1}$. This agrees well with the accretion rates commonly estimated for the two classes: $\sim 10^{-10}$ and $\sim 10^{-8}\,{\rm M}_\odot\,{\rm yr}^{-1}$, respectively (Patterson 1984; Knigge, Baraffe & Patterson 2011).

Can we therefore deduce accretion rate from spin-up measurements? Not really; it is too sensitive to magnetic moment, the slow-rotator assumption, and the variations in $\dot{P}$ sometimes seen on time-scales of decades (e.g. FO Aqr Patterson et al. 1998). But the agreement found here suggests that it is not a doomed enterprise. The enormous spread in $\dot{P}$ and P supplies a powerful lever arm to this method.

6 SUMMARY

(1) We report long photometric campaigns on the IP RX2133, covering all seasons from 2010 to 2016. We find that the light curves are dominated by a strong modulation of semi-amplitude 73 ± 8 mmag and mean periodicity of 0.28023(13) d, or 6.726(3) h. This value is 6.1 ± 0.1 per cent shorter than the orbital period of the binary, 7.13834(12) h. We interpret this wave as a negative superhump associated with the nodal precession of the accretion disc.

(2) We do not find a photometric signal at the expected nodal precession frequency, with an upper limit of ∼0.02 mag. This signal is displayed by some negative superhumpers, and is usually attributed to modulations due to varying projected surface area of the tilted accretion disc during the precession cycle. Its absence in RX2133 may signify a binary of low inclination.

(3) The mean spin period of the white dwarf is 570.825(8) s. The semi-amplitude of the spin signal is 47 ± 3 mmag, and its waveform is quite stable and nearly sinusoidal.

(4) We detect in all seasons a signal at the lower orbital side-band ($f_{\rm sp} - f_{\rm orb}$) with a semi-amplitude of 15 ± 3 mmag. Although we do not find direct detection of the orbital frequency in the power spectra, the orbital side-band provides an indirect determination of the orbital period. The inferred value of 7.1384(14) h is consistent with the period established from radial velocities.

(5) We also find low-amplitude signals in the high-frequency domain associated with combinations of the form $(f_{\rm sp} - f_{\rm orb}) \pm f_{\rm nsh}$. Presumably, they result from amplitude modulation of the orbital side-band on the superhump signal.

(6) We provide an accurate ephemeris for the spin pulse based on 239 timings of maximum light well spread over the 7 yr spanned by our observations. We find that the white dwarf spins up at a rate of $\dot{P} = -3.41(2)$ ms yr^{-1}, and the corresponding time-scale of spin period variations, $|P/\dot{P}| = 0.17 \times 10^6$ yr, is the shortest among the spin-up IP stars.

(7) Our observations of RX2133 bring the number of IPs with well-measured spin-up rates to 16, including four with well-established limits. From a preliminary analysis, we find that they seem to form two distinct classes: those with short $P_{\rm orb}$ have extremely stable spin periods ($\dot{P} \approx 0$), while those with longer $P_{\rm orb}$ have non-constant spin periods ($\dot{P} \neq 0$), with the boundaries between both groups being approximately determined by the period gap in CVs. We argue that this distinction may be a consequence of the difference in accretion rates on the two sides of the period gap.

[3] We exclude GK Per, since its $\dot{P}$ value is not based on cycle-counting and is therefore less reliable than the rest of $\dot{P}$ values.

Downloaded from https://academic.oup.com/mnras/article-abstract/467/1/428/2908342
by Biblioteca Universitaria de Huelva user
on 11 June 2018

ACKNOWLEDGEMENTS

We thank the National Science Foundation for support of this research (AST-1211129 and AST-1615456), and NASA through HST-G0-13630. EdM acknowledges financial support from the Ministerio de Educación, Cultura y Deporte (Spain) under the Mobility Program Salvador de Madariaga (PRX15/00521).

REFERENCES

Anzolin G., de Martino D., Falanga M., Mukai K. Bonnet-Bidaud J.-M., Mouchet M., Terada Y., Ishida M., 2009, A&A, 501, 1047
Araujo-Betancor S. et al., 2005, A&A, 430, 629
Armstrong E. et al., 2013, MNRAS, 435, 707
Barrett P., O'Donoghue D., Warner B., 1988, MNRAS, 233, 759
Bonnet-Bidaud J.-M., Motch C., Mouchet M., 1985, A&A, 143, 313
Bonnet-Bidaud J.-M., Mouchet M., de Martino D., Silvotti R., Motch C., 2006, A&A, 445, 1037
Butters O. W., Barlow E. J., Norton A. J., Mukai K., 2007, A&A, 475, L29
Butters O. W., Norton A. J., Hakala P., Mukai K., Barlow E. J., 2008, A&A, 487, 271
de Martino D. et al., 2006, in Wilson A., ed., ESA SP-604: The X-ray Universe 2005. ESA, Noordwijk, p. 261
de Miguel E. et al., 2012, Soc. Astron. Sci. Ann. Symp., 31, 79
de Miguel E. et al., 2016, MNRAS, 457, 1447
Gänsicke B. et al., 2005, MNRAS, 361, 141
Ghosh P., Lamb F. K., 1979, ApJ, 23, 296
Gies D. R. et al., 2013, ApJ, 775, 64
Harvey D., Skillman D. R., Patterson J., Ringwald F. A., 1995, PASP, 107, 551
Hellier C., 1997, MNRAS, 288, 817
Hellier C., Sproats L. N., 1992, IBVS, 3724
Hirose M., Osaki Y., 1990, PASJ, 42, 135
Kaluzny J., Semeniuk I., 1988, IBVS, 3145
Katajainen S., Butters O. W., Norton A. J., Lehto H. J., Piirola V., 2007, A&A, 475, 1011
Kato T., Maehara H., 2013, PASJ, 65, 76
Kato T., Osaki Y., 2013a, PASJ, 65, 115
Kato T., Osaki Y., 2013b, PASJ, 65, L13
Kato T. et al., 2014a, PASJ, 66, 30
Kato T. et al., 2014b, PASJ, 66, 90
Kemp J., Patterson J., Thorstensen J. R., Fried R. E., Skillman D. R., Billings G., 2002, PASP, 114, 623
Knigge C., Baraffe I., Patterson J., 2011, ApJS, 194, 28
Kozhevnikov V. P., 2015, New Astron., 41, 59
Lenz P., Breger M., 2005, Commun. Asteroseismol., 146, 53
Lubow S. H., 1991, ApJ, 381, 268
Mauche C. W., 2004, in Vrielmann S., Cropper M., eds, ASP Conf. Ser. Vol. 315, Magnetic Cataclysmic Variables. Astron. Soc. Pac., San Francisco, p. 120
Mauche C. W., Brickhouse N. S., Hoogerwerf R., Luna G. J. M., Mukai K., Sterken C., 2009, Inf. Bull. Var. Stars, 5876
Montgomery M. M., 2009, ApJ, 705, 603
Motch C. et al., 1998, A&AS, 132, 341
Mukadam A. S. et al., 2016, ApJ, 821, 14M
Ohshima T. et al., 2012, PASJ, 64, L3
Ohshima T. et al., 2014, PASJ, 66, 67
Osaki Y., Kato T., 2013a, PASJ, 65, 50
Osaki Y., Kato T., 2013b, PASJ, 65, 95
Patterson J., 1979, ApJ, 233, L13
Patterson J., 1984, ApJS, 54, 443
Patterson J., 1994, PASP, 106, 209
Patterson J., Price C. M., 1981, ApJ, 243, L83
Patterson J., Robinson E. L., Nather R. E., 1978, ApJ, 224, 570
Patterson J. et al., 1998, PASP, 110, 415
Patterson J. et al., 2004, PASP, 116, 516
Patterson J. et al., 2005, PASP, 117, 1204
Patterson J. et al., 2011, PASP, 123, 130
Pavlenko E. P., Voloshina I. B., Andreev M. V., Shugarov S. Yu., Baklanov A. V., Antonyuk O. I., Parakhin N. A., Samsonov D. A., Metlov V. G., 2010, Astron. Rep., 54, 6
Pavlenko E. P., Sosnovskij A. A., Katysheva N. A., Kato T., Littlefield K., 2016, Afz, 59, 304
Ringwald F. A., Velasco K., Roveto J. J., Meyers M. E., 2012, New Astron., 17, 433
Ritter H., 1985, A&A, 148, 207
Scaringi S. et al., 2011, A&A, 530, A6
Shugarov S. Y. et al., 2005, in Hameury J.-H., Lasota J.-P., eds, ASP Conf. Ser. Vol. 330, The Astrophysics of Cataclysmic Variables and Related Objects. Astron. Soc. Pac., San Francisco, p. 495
Thorstensen J. R., Peters C. S., Skinner J. N., 2010, PASP, 122, 1285
Vogt N., 1974, A&A, 36, 369
Warner B., 1975, MNRAS, 170, 219
Warner B., 1986, MNRAS, 219, 347
Whitehurst R., 1988, MNRAS, 232, 35
Whitehurst R., King A., 1991, MNRAS, 249, 95

SUPPORTING INFORMATION

Supplementary data are available at *MNRAS* online.

spin-timings.txt

Please note: Oxford University Press is not responsible for the content or functionality of any supporting materials supplied by the authors. Any queries (other than missing material) should be directed to the corresponding author for the article.

This paper has been typeset from a TEX/LATEX file prepared by the author.

Downloaded from https://academic.oup.com/mnras/article-abstract/467/1/428/2908342
by Biblioteca Universitaria de Huelva user
on 11 June 2018